

HENet: Hybrid Encoding for End-to-end Multi-task 3D Perception from Multi-view Cameras

Zhongyu Xia¹ Zhiwei Lin¹ Xinhao Wang¹ Yongtao Wang^{1*}
 Yun Xing² Shengxiang Qi² Nan Dong² Ming-Hsuan Yang³

¹ Wangxuan Institute of Computer Technology, Peking University

² Chongqing Changan Automobile Co., Ltd.

³ University of California, Merced

{xiazhongyu, zwlin, wangxinhao, wyt}@pku.edu.cn,
 dongnan1@changan.com.cn, mhyang@ucmerced.edu

Abstract. Three-dimensional perception from multi-view cameras is a crucial component in autonomous driving systems, which involves multiple tasks like 3D object detection and bird’s-eye-view (BEV) semantic segmentation. To improve perception precision, large image encoders, high-resolution images, and long-term temporal inputs have been adopted in recent 3D perception models, bringing remarkable performance gains. However, these techniques are often incompatible in training and inference scenarios due to computational resource constraints. Besides, modern autonomous driving systems prefer to adopt an end-to-end framework for multi-task 3D perception, which can simplify the overall system architecture and reduce the implementation complexity. However, conflict between tasks often arises when optimizing multiple tasks jointly within an end-to-end 3D perception model. To alleviate these issues, we present an end-to-end framework named HENet for multi-task 3D perception in this paper. Specifically, we propose a hybrid image encoding network, using a large image encoder for short-term frames and a small image encoder for long-term temporal frames. Then, we introduce a temporal feature integration module based on the attention mechanism to fuse the features of different frames extracted by the two aforementioned hybrid image encoders. Finally, according to the characteristics of each perception task, we utilize BEV features of different grid sizes, independent BEV encoders, and task decoders for different tasks. Experimental results show that HENet achieves state-of-the-art end-to-end multi-task 3D perception results on the nuScenes benchmark, including 3D object detection and BEV semantic segmentation. The source code and models will be released at <https://github.com/VDIGPKU/HENet>.

1 Introduction

Efficient and accurate perception of the surrounding environment from multi-view cameras is essential for the autonomous driving system, which serves as the

* Corresponding author.

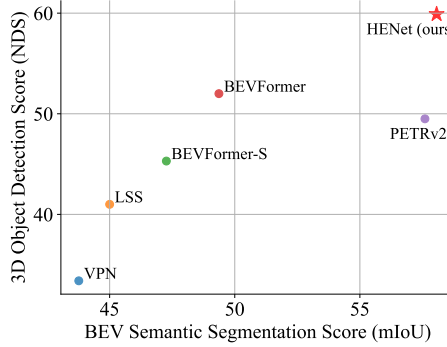


Fig. 1: Comparisons of end-to-end multi-task results on nuScenes val set.

basis for subsequent trajectory prediction and motion planning tasks. A desirable 3D perception system should handle several tasks simultaneously, including 3D object detection and bird’s-eye-view (BEV) semantic segmentation. There has been an increasing emphasis on end-to-end multi-task frameworks, as such systems have the potential to streamline the overall architecture and alleviate implementation complexities.

However, end-to-end multi-task 3D perception faces the following challenges. First, when designing high-performance camera-based 3D perception models, researchers usually exploit techniques like higher-resolution images, longer temporal inputs, and larger image encoders to improve 3D perception accuracy. Nevertheless, *simultaneously employing these techniques on a single perception model would result in a formidable cost during training*. To alleviate this issue, a few works [32, 46] store past information in memory, which has disadvantages such as inconsistency of temporal features and inefficiency of data augmentations. Therefore, many of the latest methods [26, 37, 44, 53] do not adopt this strategy, but recompute features of past frames, albeit at the expense of training costs.

Second, to process long-term temporal inputs, many works [11, 17, 18] directly sum or concatenate the features from different frames in BEV along the channel dimension, showing unsatisfactory perception performance with longer time sequence. The reason is that *the features of the moving objects are misaligned and scattered across large regions in BEV along their trajectories in different frames*. Therefore, it is necessary to introduce dynamic alignment mechanisms [28, 37] for location correction of moving objects.

Third, for end-to-end multi-task learning, existing works [8, 19, 28] use a shared encoding network with multiple decoders for different tasks. However, experimental results in these works show that *jointly learning multiple tasks in the end-to-end fashion is often sub-optimal, i.e.,* the performance of each task in multi-task learning is lower than standing-alone training. To alleviate this issue, some works [28] propose adjusting the loss weight for each task, but there is no comprehensive analysis of why a conflict exists between the tasks.

In this paper, we present HENet, an end-to-end multi-task 3D perception framework for multi-view cameras. To integrate large image encoders, high-resolution images, and long-term inputs, we propose a hybrid image encoding network that adopts different resolutions and image encoders for different frames. Specifically, we use high-resolution inputs, a large image backbone, and a complex perspective transformation network for short-term frames to produce high-precision BEV features. For long-term frames, low-resolution inputs are chosen, and a small image backbone and a simple perspective transformation network are employed to generate BEV features efficiently. The proposed hybrid image encoding network can be easily incorporated into existing perception models. Then, we introduce a temporal integration module to align and fuse the BEV features from multi-frames dynamically. Specifically, in this module, we present a temporal backward and forward process with adjacent frame fusion modules (AFFM) to aggregate BEV features, addressing the problem of aligning moving objects with the attention mechanism. Finally, we deeply analyze the conflict between 3D object detection and BEV semantic segmentation in multi-task learning and find the critical problem is that different tasks prefer different BEV feature grid sizes. Based on this observation, we select BEV features of different grid sizes for different tasks. The selected features are sent to independent BEV encoding networks and task decoders to alleviate the task conflicts further to obtain the final 3D perception results.

The main contributions of this work are summarized as follows:

- We present an end-to-end multi-task 3D perception framework with a hybrid image encoding network to take advantage of high-resolution images, long-term inputs, and large image encoders with a smaller training cost.
- We introduce a temporal integration module based on the attention mechanism to fuse the multi-frame BEV features and enable the dynamic inter-frame alignment for moving objects.
- We analyze the task conflicts in end-to-end multi-task learning and propose a feature size selection and independent feature encoding to alleviate this problem.
- We achieve state-of-the-art results in end-to-end multi-task learning on nuScenes, including 3D object detection and BEV semantic segmentation tasks.

2 Related Work

2.1 Multi-View 3D Object Detection

Three-dimensional object detection from images is a crucial task in multi-task 3D perception. Early approaches focus on predicting objects directly from monocular images [2, 4, 31, 34, 36, 38–40]. Recently, multi-view cameras become the default sensors for autonomous driving cars, which can provide more information. Based on the type of view transformations, current multi-view 3D object detection works can be divided into two categories, *i.e.*, BEV-based methods [5, 9, 11, 12, 14, 17–19, 32, 42, 44, 53] and sparse query methods [13, 24–28, 37, 41, 46, 49].

BEV-based Methods. BEVDet [12] utilizes Lift-Splat-Shoot (LSS) [33] to generate the BEV feature from multi-view image features with depth prediction. To address the issue of inaccurate depth estimation in BEVDet [12], BEVDepth [18] introduces extrinsic parameters for the depth prediction network and adds additional depth supervision from LiDAR point clouds. BEVDet4D [11] incorporates temporal information by aligning BEV features from different frames through ego-vehicle transformations. Based on BEVDepth [18], BEVStereo [17] and STS [42] present temporal stereo techniques to improve depth prediction further. To gather long-term temporal information, BEVFormer [19] and Polarformer [14] regard the BEV feature as queries and utilize cross-attention to aggregate information from all past frames. BEVFormerv2 [44] further introduces perspective space supervision to enhance the performance of BEVFormer. SOLOFusion [32] proposes to first fuse adjacent short-term series BEV features and then fuse long-term series. HoP [53] designs a historical object prediction module, which can be easily plugged into any temporal 3D object detectors. AeDet [5] proposes azimuth-equivariant convolution operations and anchors to unify the BEV representation in different azimuths.

Sparse Query Methods. As a pioneer in sparse query method, DETR3D [41] extends DETR [29] by utilizing a sparse 3D object query set to index features. 3D-MAN [46] designs an alignment and aggregation module to extract temporal features from the memory bank that stores information generated by a single frame detector. PETR [27] builds upon DETR3D [41] by aggregating image features with 3D position information. PETRv2 [28] introduces temporal information into 3D position embedding in PETR [27] to allow temporal alignment for object positions across different frames. Sparse4D [24] assigns and projects 4D keypoints to generate different view, scale, and timestamp features. Sparse4Dv2 [25] improves the temporal fusion module to reduce the computational complexity and enable long-term fusion. StreamPetr [37] presents an efficient intermediate representation to transfer temporal information like BEV-based methods to avoid repeated calculation of features. SparseBEV [26] designs a scale-adaptive self-attention module for query feature interaction and proposes spatiotemporal sampling and adaptive mixing to aggregate temporal features into current queries. To explore long-range detection, Far3D [13] uses a perspective-aware aggregation module to capture features of long-range objects and designs a denoising method to improve query propagation.

2.2 BEV Semantic Segmentation

Another task in multi-task 3D perception involves BEV semantic segmentation, which aims to comprehend the overall scene. Many works [7, 30, 33, 35, 45] share a common paradigm like BEVDet [12], except for different task heads. VPN [30] trains their network in a 3D graphics environment and utilizes domain adaptation techniques to transfer it for handling real-world data. M2BEV [43] adeptly transforms multi-view 2D image features into 3D BEV features in the ego vehicle coordinates. This BEV representation is paramount, as it facilitates sharing a singular encoder across diverse tasks. CVT [50] employs a cross-view attention

mechanism to implicitly learn the mapping from an individual camera view to a canonical map view representation. Each camera utilizes position embeddings dependent on its intrinsic and extrinsic calibration. HDMapNet [16] encodes image features from surrounding cameras or point clouds from LiDAR and predicts vectorized map elements in a BEV map.

2.3 End-to-end Multi-task Learning

In autonomous driving scenarios, multi-task learning, usually including 3D object detection and BEV segmentation [30, 35, 48, 52], is crucial for scene understanding. Current works often follow the joint training strategy of BEV-Former [19], which generates a unified BEV feature map for detection and segmentation tasks. PETRv2 [28] initializes two query sets for detection and segmentation tasks and sends each query set to corresponding task heads. The latest work UniAD [8] integrates three major tasks, including perception, prediction, and planning, and six sub-tasks into an end-to-end framework with query design as the connection between tasks.

These works show conflicts between tasks when combining detection and segmentation tasks. Nevertheless, no comprehensive analysis has been reported to address this issue. In this work, we make an attempt to investigate the problem of performance degradation in multi-task training of 3D object detection and BEV semantic segmentation. Most importantly, we propose an efficient multi-task 3D perception framework and an effective training strategy to alleviate this issue. Our model can achieve state-of-the-art 3D object detection and BEV segmentation results in multi-task settings.

3 Method

We illustrate the overall architecture of HENet in Figure 2. Given temporal multi-view image inputs, a hybrid image encoding network extracts their BEV features. Then, we use a temporal feature integration module to aggregate the multi-frame BEV features. Finally, we send BEV features in different grid sizes to independent BEV feature encoders and decoders for different tasks to obtain the multi-task perception results.

3.1 Hybrid Image Encoding Network

As shown in Figure 2, the hybrid image encoding network contains two image encoders with different complexity. Specifically, the first one processes short-term frames, which scales up the high-resolution inputs and sends them to an image backbone and a feature pyramid network (FPN). Then, a complex 2D-to-BEV network is applied to produce high-precision BEV features. The second image encoder handles the long-term sequences by down-sampling the inputs to low resolution and utilizing a small backbone and FPN to extract image features. Similarly, a simple 2D-to-BEV network is adopted afterward for efficient BEV

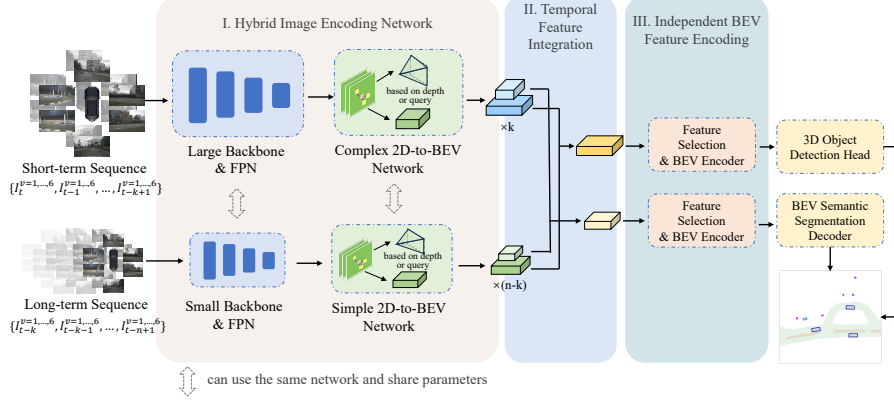


Fig. 2: Overall architecture of HENet. i) Hybrid Image Encoding Network uses image encoders of varying complexity to encode long-sequence frames and short-term images, respectively. ii) Temporal Feature Integration module based on the attention mechanism fuses multi-frame features from multiple image encoders. iii) Based on the characteristics of different tasks, we select BEV feature maps of appropriate sizes and perform independent BEV encoding for each task.

feature generation. Some parts of the two image encoders can be shared. For example, we can use the same backbone with a different 2D-to-BEV network. However, the first image encoder is more complex than the second one.

The aforementioned hybrid image encoding network can be incorporated into existing multi-view 3D object detection methods. Without loss of generality, we choose two popular BEV-based approaches, BEVDepth [18] and BEVStereo [17], as examples to show how the proposed hybrid image encoding network works. Specifically, for the first image encoder, which processes the short-term frames, we keep a high resolution for images and utilize a large backbone (*e.g.*, VoVNetV2-99 [15]) followed by FPN [22] to extract the features. Then, multiple convolution layers and EM algorithm in BEVStereo [17] are applied to generate stereo depth and frustum features. BEVPoolv2 [10] converts frustum features into multi-scale BEV features. As for the second image encoder, we first down-sample the image size for the long-term image sequences and then use a small backbone (*e.g.*, ResNet-50) followed by FPN [22] to extract the multi-view image features. After that, we adopt the simple monocular depth estimation network in BEVDepth [18] to obtain frustum features. Further, we use BEVPoolv2 [10] to transform frustum features in perspective view into multi-scale BEV features according to the camera’s intrinsic and extrinsic parameters. We select different BEV sizes for 3D object detection and BEV semantic segmentation tasks according to experiments in Section 4.4. Specifically, we utilize BEV sizes of 256x256 for the 3D object detection task and 128x128 for the BEV semantic segmentation task.

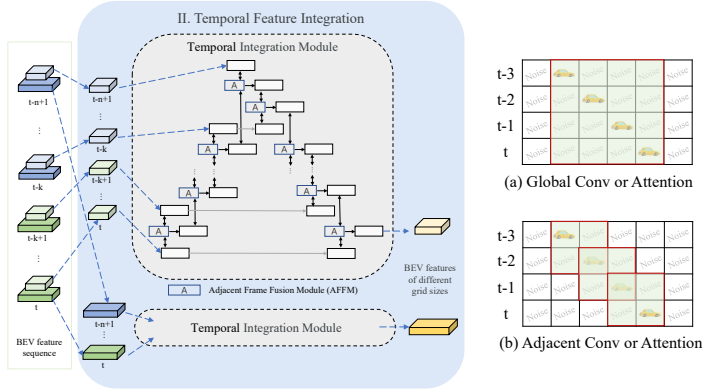


Fig. 3: Architecture of Temporal Feature Integration module. We propose the adjacent frame fusion module (AFFM) and adopt the temporal fusion strategy with temporal backward and forward processes.

Algorithm 1 Pseudo-code for Section 3.2

Input: A series of BEV features $\{f_{-n+1}, \dots, f_{-1}, f_0\}$. f_0 represents BEV feature of the current frame and f_{-i} corresponds to the i^{th} frame before f_0 .

```

for i from 0 to n-2 do
     $f_{-(i+1)} \leftarrow \text{AFFM}(f_{-i}, f_{-(i+1)})$ 
end for
for i from n-2 to 0 do
     $f_{-i} \leftarrow \text{AFFM}(f_{-(i+1)}, f_{-i})$ 
end for
return  $f_0$ 

```

3.2 Temporal Feature Integration

After generating multi-frame BEV features by the hybrid image encoding network, we adopt temporal integration modules to fuse the BEV features, as shown in Figure 3. The temporal integration module consists of a backward process and a forward process. The backward process fuses features of the current frame to past frames, while the forward process aggregates features from the past to the current frame. Algorithm 1 provides the pseudo-code of the aforementioned temporal integration process. In each process step, we employ an adjacent frame fusion module (AFFM) with a cross-attention to fuse the BEV features from two adjacent frames. Specifically, assuming the BEV features of two frames are f_i and f_j , AFFM can be formulated as:

$$\text{AFFM}(f_i, f_j) = f_j + \gamma \times \text{Avg}(\text{Attn}(\langle f_i, f_j \rangle, f_i, f_i), \text{Attn}(\langle f_i, f_j \rangle, f_j, f_j)), \quad (1)$$

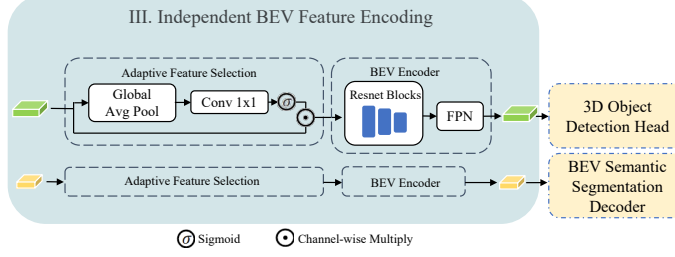


Fig. 4: Design of Independent BEV Feature Encoding. Each task decoder is provided with BEV feature maps in different grid sizes through independent adaptive feature selection and BEV encoding.

where $\text{Avg}(\cdot)$ represents the average operator, γ is a learnable scaling parameter, $\langle \cdot, \cdot \rangle$ denotes concatenation, and $\text{Attn}(\cdot, \cdot, \cdot)$ is the attention module:

$$\text{Attn}(q, k, v) = \text{softmax}\left(\frac{qk^\top}{\sqrt{d}}\right)v. \quad (2)$$

In the backward process, $j = i - 1$, while in the forward process, $j = i + 1$.

As shown in Figure 3, using adjacent attention will introduce less noise than directly applying global attention or convolution across all frames. With adjacent attention, AFFM can align the features of moving objects and avoid fusing redundant background information. Besides, the attention mechanism allows us to adopt AFFM to both BEV-based and sparse query methods.

3.3 Independent BEV Feature Encoding

Based on our empirical analysis in Section 4.4, different tasks prefer different sizes of BEV features. Thus, after obtaining the fused multi-scale BEV features, we first assign different sizes of BEV features to other tasks. We then encode the BEV feature for each task independently. Inspired by BEVFusion [21], the proposed encoding process comprises adaptive feature selection and BEV encoding.

Specifically, the adaptive feature selection $f_{\text{adaptive}}(\cdot)$ applies a simple channel attention module to select important features as follows:

$$f_{\text{adaptive}}(\mathbf{F}) = \sigma(\mathbf{W}f_{\text{avg}}(\mathbf{F})) \cdot \mathbf{F}, \quad (3)$$

where $\mathbf{F} \in \mathbb{R}^{X \times Y \times C}$ is the BEV features, \mathbf{W} denotes linear transform matrix, f_{avg} indicates the global average pooling, and σ represents the Sigmoid function. For the BEV encoder, we adopt three ResNet [6] residual blocks and a simple FPN [22] following existing BEV-based methods [11, 18] to perform local feature integration on the BEV feature map. Notably, the adaptive feature selection and BEV encoders for different tasks share the same architecture but have different weights.

3.4 Decoders and Losses

We adopt Centerpoint [47] as the 3D object detection decoder and SegNet [1] as the BEV semantic segmentation decoder. The classification and regression loss of Centerpoint [47] is represented by \mathcal{L}_{cls} and \mathcal{L}_{bbox} . We use focal loss [23] for the BEV semantic segmentation task. The loss functions for vehicles, drivable areas, and lane lines are denoted as \mathcal{L}_{segveh} , $\mathcal{L}_{segarea}$, and \mathcal{L}_{segdiv} , respectively.

The final loss function is defined as

$$\begin{aligned} \mathcal{L} = & \alpha_{depth} \mathcal{L}_{depth} + \alpha_{cls} \mathcal{L}_{cls} + \alpha_{bbox} \mathcal{L}_{bbox} + \\ & \alpha_{segveh} \mathcal{L}_{segveh} + \alpha_{segarea} \mathcal{L}_{segarea} + \alpha_{segdiv} \mathcal{L}_{segdiv}, \end{aligned} \quad (4)$$

where \mathcal{L}_{depth} is a binary cross entropy loss for depth estimation and α is the loss weight.

4 Experiments

4.1 Implementation Details

We train HENet in end-to-end manner for multi-tasks, including 3D object detection and BEV semantic segmentation in the same way as LSS [33]. We choose VovNet-99 [15, 31] with 896×1600 image resolution for the large image encoder and select ResNet-50 [6] with 256×704 image resolution for the small image encoder, respectively. For the input temporal sequence, we set short-term frame number $k = 2$ and long-term frame number $n = 9$. The weights of the hybrid image encoding network are initialized from pre-trained 3D detectors. As analyzed in Sec.4.4, we choose BEV grid sizes of 0.4m (256×256 BEV size) and 0.8m (128×128 BEV size) for 3D object detection and BEV semantic segmentation, respectively. The end-to-end multi-task models are trained for 60 epochs without CBGS. Besides, to further compare HENet with some single-task methods, we train the single 3D object detection models of HENet for 12 epochs with CBGS [51].

4.2 Dataset and Metrics

We evaluate our model on the nuScenes [3] dataset, a large-scale autonomous driving dataset containing 1,000 driving scenes (700 for training, 150 for validation, and 150 for testing), including cities, highways, and rural roads. Each scene contains various objects, such as vehicles, pedestrians, and bicycles.

For 3D object detection evaluation, NuScenes provides a set of evaluation metrics, including mean Average Precision (mAP) and five true positive (TP) metrics: ATE, ASE, AOE, AVE, and AAE for measuring translation, scale, orientation, velocity, and attribute errors respectively. The overall performance is measured by the nuScenes Detection Score (NDS), which is the composite of the above metrics. For BEV semantic segmentation, we use mean intersection over union (mIoU) as the metric following the settings of LSS [33].

Table 1: Comparison of end-to-end multi-task learning on the nuScenes val set. Time/E represent the training time per epoch with FP32 on 8×A800 GPUs. mIoU_v, mIoU_a, and mIoU_d represent the mIoU for vehicles, drivable area, and lane & road divider, respectively.

Methods	Backbone	Input Size	Frames	Time/E	NDS↑ mAP↑	mIoU↑ mIoU _v ↑ mIoU _a ↑ mIoU _d ↑
VPN [30]	ResNet50	900×1600	1	-	33.4 25.7	43.8 37.3 76.0 18.0
LSS [33]	ResNet50	900×1600	1	-	41.0 34.4	45.0 42.8 73.9 18.3
BEVFormer-S [19]	ResNet101-DCN	900×1600	1	-	45.3 38.0	47.3 44.4 77.6 19.8
BEVFormer [19]	ResNet101-DCN	900×1600	5	213min	52.0 41.2	49.4 46.7 77.5 23.9
UniAD [8]	ResNet101	900×1600	6	253min	49.9 38.2	- - 69.1 25.7
HENet (Ours)	ResNet101 & ResNet50	640×1152&256×704	2 & 3	60min	56.4 47.1	53.9 44.5 77.0 40.1
PETRv2 [28]	V2-99	640×1600	2	75min	49.5 40.1	57.6 49.4 79.1 44.3
HENet (Ours)	V2-99 & ResNet50	640×1152 & 256×704	2	58min	58.0 48.7	56.9 47.6 80.2 42.8
HENet (Ours)	V2-99 & ResNet50	640×1152 & 256×704	2 & 7	71min	59.9 49.9	58.0 49.5 81.3 43.4

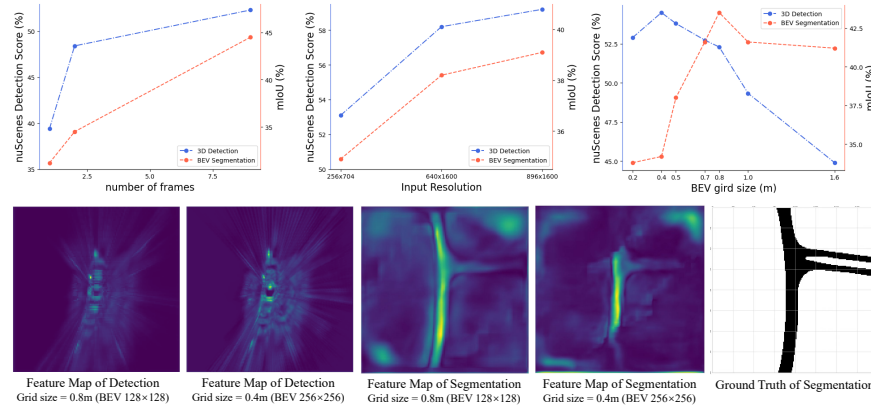


Fig. 5: Analysis of similarities and differences between 3D object detection and BEV semantic segmentation. Experimental results show that each task has a suitable BEV grid size. The suitable grid size of BEV Semantic Segmentation is larger than 3D Object Detection.

4.3 Main Results

We compare the proposed HENet with previous end-to-end multi-task models on the nuScenes val sets in Table 1 and Figure 1. HENet shows favorable multi-task performance and achieves state-of-the-art results. Specifically, HENet outperforms BEVFormer [19] by 7.9 NDS and 8.7 mAP on the 3D object detection task and 8.6 mIoU on the BEV semantic segmentation task. As for PETRv2 [28], which shows excellent BEV semantic segmentation performance, our models surpass it by 10.4 NDS on the 3D object detection task while keeping competitive performance on the BEV semantic segmentation task.

In addition, we compare the training time per epoch (with the same batch size) with these methods. HENet outperforms all other methods with less training time, showing the proposed HENet is more efficient. Moreover, HENet can use more frames to improve performance, while other methods, like PETRv2, cannot use 9 frames due to the limitation of GPU memory.

Table 2: Comparison of 3D object detection results on the nuScences val set. * indicates the result is benefited from the perspective pre-training. † indicates using one temporal frame information. ‡ denotes integrating two or more temporal frames. The best and second best results are marked in red and blue.

Methods	Backbone	Input Size	NDS↑	mAP↑	mATE↓	mASE↓	mAOE↓	mAVE↓	mAAE↓
BEVDet [12]	ResNet50	256×704	37.9	29.8	0.725	0.279	0.589	0.860	0.245
BEVDet4D [11]†	ResNet50	256×704	45.7	32.2	0.703	0.278	0.495	0.354	0.206
PETRv2 [28]†	ResNet50	256×704	45.6	34.9	0.700	0.275	0.580	0.437	0.187
BEVstereo [17]†	ResNet50	256×704	50.0	37.2	0.598	0.270	0.438	0.367	0.190
SOLOFusion [32]‡	ResNet50	256×704	53.4	42.7	0.567	0.274	0.511	0.252	0.181
Sparse4Dv2 [25]‡	ResNet50	256×704	53.9	43.9	0.598	0.270	0.475	0.282	0.179
StreamPETR [37]‡	ResNet50	256×704	54.0	43.2	0.581	0.272	0.413	0.295	0.195
SparseBEV [26]‡	ResNet50	256×704	54.5	43.2	0.606	0.274	0.387	0.251	0.186
HENet (Ours)‡	ResNet50	256×704	55.4	43.7	0.512	0.262	0.367	0.285	0.213
PETR [27]*	ResNet101-DCN	512×1408	44.1	36.6	0.717	0.267	0.412	0.834	0.190
BEVDepth [18]*‡	ResNet101	512×1408	53.5	41.2	0.565	0.266	0.358	0.331	0.190
BEVFormer [19]*‡	ResNet101-DCN	900×1600	51.7	41.6	0.673	0.274	0.372	0.394	0.198
HoP-BEVFormer [53]*‡	ResNet101-DCN	512×1408	55.8	45.4	0.565	0.265	0.327	0.337	0.194
StreamPETR [37]*‡	V2-99	320×800	57.1	48.2	0.569	0.262	0.315	0.257	0.199
SOLOFusion [32]*‡	ResNet101	512×1408	58.2	48.3	0.503	0.264	0.381	0.246	0.207
SparseBEV [26]*‡	ResNet101	512×1408	59.2	50.1	0.562	0.265	0.321	0.243	0.195
Far3D [13]*‡	ResNet101	512×1408	59.4	51.0	0.551	0.258	0.372	0.238	0.195
HENet (Ours)*‡	V2-99 & ResNet50	640×1152 & 256×704	59.9	50.2	0.465	0.261	0.335	0.267	0.197

4.4 Analysis of Conflict in End-to-end Multi-task 3D Perception

To analyze the conflict between 3D object detection and BEV semantic segmentation tasks, we first conduct experiments on single tasks to find the optimal configuration of training and models, including the resolution of the input images, the number of temporal frames, and the BEV feature grid sizes. As shown in the upper part of Figure 5, we observe that the results of 3D object detection and BEV semantic segmentation tasks are consistently improved when the input resolutions and the number of temporal frames increase. However, for BEV feature grid size, we find that different tasks prefer different BEV grid sizes. We conjecture this inconsistency can be attributed to the tasks’ characteristics. The 3D object detection task focuses on localizing local foreground objects. In contrast, the BEV semantic segmentation task is required to comprehensively understand the large-scale scene, including lane lines and roads. As shown in the bottom of Figure 5, the BEV feature of detection is local highlighting, while the segmentation feature shows more activated regions globally. Therefore, when the BEV feature grid size is too small, the BEV semantic segmentation task suffers from aggregating local features and cannot capture global information for the whole scene understanding. By contrast, larger BEV features can provide more local details for the 3D object detection task.

4.5 Single Task Results

Considering that many works on 3D perception only predict single-task results, we conduct experiments on single tasks and compare the results of HENet with these task-specific models. Through this comparison, we illustrate the superiority of our Hybrid Image Encoding Network and Temporal Feature Integration, and further demonstrate the effectiveness of HENet.

Table 3: Comparison of 3D object detection results on nuScences test set.
 The best and second best results are marked in red and blue. †uses future frames. ‡uses test-time augmentation.

Methods	Backbone	Input Size	NDS↑	mAP↑	mATE↓	mASE↓	mAOE↓	mAVE↓	mAAE↓
BEVDet4D [11]	Swin-B	900×1600	56.9	45.1	0.511	0.241	0.386	0.301	0.121
PolarFormer [14]	V2-99	900×1600	57.2	49.3	0.556	0.256	0.364	0.439	0.127
PETRv2 [28]	V2-99	640×1600	58.2	49.0	0.561	0.243	0.361	0.343	0.120
Hop-BEVFormer [53]	V2-99	900×1600	60.3	51.7	0.501	0.245	0.346	0.362	0.105
BEVDepth [18]	ConvNeXt-B	640×1600	60.9	52.0	0.445	0.243	0.352	0.347	0.127
BEVStereo [17]	V2-99	640×1600	61.0	52.5	0.431	0.246	0.358	0.357	0.138
SOLOFusion [32]	ConvNeXt-B	640×1600	61.9	54.0	0.453	0.257	0.376	0.276	0.148
AeDet [5]	ConvNeXt-B	640×1600	62.0	53.1	0.439	0.247	0.344	0.292	0.130
BEVFormerV2 [44]	InternImage-B	640×1600	62.0	54.0	0.488	0.251	0.335	0.302	0.122
FB-BEV [20]	V2-99	640×1600	62.4	53.7	0.439	0.250	0.358	0.270	0.128
StreamPETR [37]	V2-99	640×1600	63.6	55.0	0.479	0.239	0.317	0.241	0.119
SparseBEV [26]	V2-99	640×1600	63.6	55.6	0.485	0.244	0.332	0.246	0.117
Sparse4Dv2 [25]	V2-99	640×1600	63.8	55.6	0.462	0.238	0.328	0.264	0.115
HENet (Ours)	V2-99 & ResNet50	640×1152 & 256×704	63.8	57.5	0.432	0.242	0.368	0.320	0.129
BEVFormerV2 [44] †	InternImage-XL		64.8	58.0	0.448	0.262	0.342	0.238	0.128
BEVDet-Gamma [12] ‡†	Swin-B		66.4	58.6	0.375	0.243	0.377	0.174	0.123
SparseBEV [26] †	V2-99		67.5	60.3	0.425	0.239	0.311	0.172	0.116
StreamPETR-Large [37]	ViT-L		67.6	62.0	0.470	0.241	0.258	0.236	0.134
Hop [53] †	ViT-L		68.5	62.4	0.367	0.249	0.353	0.171	0.131
Far3D [13]	ViT-L		68.7	63.5	0.432	0.237	0.278	0.227	0.130
HENet_Sp (Ours) †	ViT-L & V2-99		70.7	64.5	0.402	0.235	0.237	0.155	0.129

3D Object Detection Results. We present the results of HENet for single 3D object detection task on the nuScenes `val` and `test` sets in Table 2 and 3, respectively. As shown in Table 2, HENet surpasses all multi-view camera 3D object detection methods under different backbone and input resolution configurations, demonstrating the effectiveness of the proposed hybrid image encoding network and temporal feature integration module.

For online evaluation, Table 3 shows HENet achieves state-of-the-art 3D object detection results. To further demonstrate the effectiveness of HENet, we choose SparseBEV [26] as the baseline and incorporate it with HENet. We successfully implemented Hybrid Image Encoding of short-term ViT-L and long-term V2-99, proving the effectiveness of the Hybrid Image Encoding Network in reducing training costs. We achieve new state-of-the-art 3D detection results with 70.7 NDS and 64.5 mAP on nuScenes leaderboard (detection task/vision track).

BEV Semantic Segmentation Results. We present the results of HENet for single BEV semantic segmentation task on the nuScenes `val` sets in Table 4. HENet obtain competitive results compared to existing methods.

It is worth mentioning that compared with single-task performance, the end-to-end multi-task performance of HENet only drops 0.3 mAP and 0.8 mIOU for the 3D object detection task and the BEV semantic segmentation task, respectively. These results indicate the effectiveness of the independent BEV feature encoding design, as well as the use of different BEV grid sizes for addressing multi-task conflict problems.

Table 4: Comparison of BEV semantic segmentation results on nuScences val set. The best and second best results are marked in red and blue.

Methods	Backbone	mIoU	mIoU _{veh} ↑	mIoU _{area} ↑	mIoU _{div} ↑
VPN [30]	ResNet50	42.7	31.8	76.9	19.4
LSS [33]	ResNet50	46.5	41.7	77.7	20.0
BEVFormer [19]	ResNet101-DCN	50.2	44.8	80.1	25.7
FIERY [7]	ResNet-101	-	38.2	-	-
M2BEV [43]	ResNeXt-101	-	-	77.2	40.5
PETRv2 [28]	V2-99	60.3	46.3	85.6	49.0
HENet (Ours)	V2-99 & ResNet50	58.8	51.6	82.3	42.4

Table 5: Ablation of Hybrid Image Encoding Network on Detection Task. ‘Time’ denotes the overall training time. ‘BS’ indicates the batch size. FPS is measured on a single RTX3090 with FP32. Training cost (GPU memory and time) is estimated on 8×Tesla A800 GPUs with FP32.

	Model	Backbone	Input	Frames	NDS mAP	FPS	GPU memory	Time
A	BEVDepth4D	R50	256×704	9 frames	53.8	40.9	19.1 14.1G / BS=16	16h
B	BEVStereo	V2-99	640×1152	2 frames	58.2	48.0	4.52 37.0G / BS=16	48h
C	BEVStereo	V2-99	896×1600	2 frames	59.2	50.0	2.69 68.4G / BS=16	96h
A+B	Model Ensemble	-	-	-	57.3	46.4	3.53	-
A+B	HENet w/o AFFM	V2-99 & R50	640×1152 & 256×704	2 & 7 frames	59.2	49.9	3.71 42.3G / BS=16	27h
A+B	HENet	V2-99 & R50	640×1152 & 256×704	2 & 7 frames	59.9	50.2	3.65 43.5G / BS=16	27h
D	BEVDepth4D	R18	640×1152	2 frames	48.6	34.8	14.3 31.2G / BS=64	14h
E	BEVDepth4D	R18	256×704	9 frames	48.6	34.9	21.7 22.9G / BS=64	14h
F	BEVDepth4D	R18	640×1152	9 frames	51.2	39.2	14.1 43.5G / BS=64	44h
D+E	Model Ensemble	-	-	-	48.9	35.2	7.93	-
D+E	HENet	R18 & R18	640×1152 & 256×704	2 & 7 frames	52.1	39.8	8.91 41.3G / BS=64	13h

4.6 Ablation

We also conduct ablation studies for each proposed module on nuScenes val set. In the following experiment, we adopt BEVDepth4D [18] as the small image encoder and BEVStereo [17] as the large image encoder.

Hybrid Image Encoding Network. To demonstrate the effectiveness of the proposed hybrid image encoding network, we compare HENet with the two baseline methods and their ensemble model. As shown in Table 5, by combining with BEVDepth4D [18] and BEVStereo [17] through hybrid image encoding, HENet can significantly improve the 3D object detection performance. Compared to increasing resolution (model C), Hybrid Image Encoding Network can achieve higher accuracy with faster inference speed and lower training costs. Compared to increasing the frame number (model F), Hybrid Image Encoding Network can achieve higher accuracy with lower training costs. Notably, ensembling the results of the two baselines by NMS decreases the overall performance since the weaker BEVDepth4D [18] introduces many false positive detection results.

For better comparison, we provide a multi-task ablation study, as shown in Table 6.

We also provide the visualization of the detection results in Figure 6. It can be seen that, due to motion or occlusion, some objects or scenes (as shown in the blue boxes) require a longer time sequence. Besides, high-resolution and sophisticated depth estimation methods benefit the perception of difficult objects and

Table 6: Ablation of Hybrid Image Encoding Network on Multi-task.

	Model	Backbone	Input	Frames	NDS	mIoU
A	BEVDepth4D	R50	256×704	9 frames	53.0	51.5
B	BEVStereo	V2-99	640×1152	2 frames	58.0	55.8
C	BEVStereo	V2-99	896×1600	2 frames	58.9	56.7
A+B	HENet w/o AFFM	V2-99 & R50	640×1152 & 256×704	2 & 7 frames	59.0	56.9
A+B	HENet w/ AFFM	V2-99 & R50	640×1152 & 256×704	2 & 7 frames	59.9	58.0

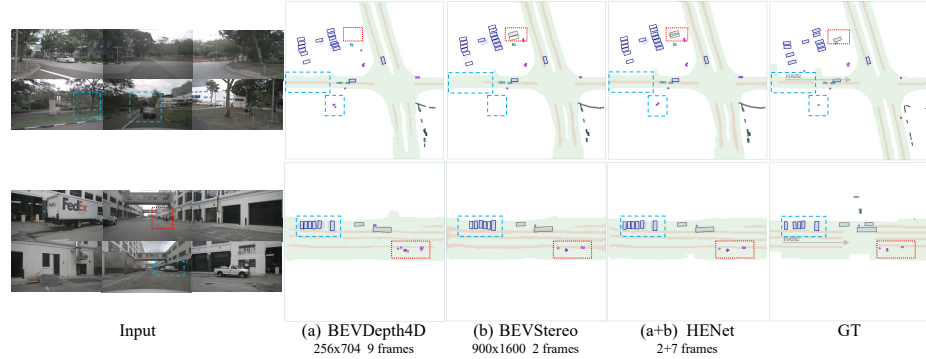


Fig. 6: Visualization results of HENet and baselines on end-to-end multi-tasking. From left to right, we show multi-view image inputs, results of BEVDepth4D, BEVStereo, and HENet (BEVDepth4D + BEVStereo), and the ground truth. The proposed HENet estimates occluded objects better through long-term information and has more accurate predictions through high-resolution information.

scenes (as shown in the red boxes). HENet can effectively combine the advantages of long-time sequence, high-resolution, and sophisticated depth estimation.

Temporal Feature Integration. Table 7 compares the results between different types of temporal feature integration methods.

Our adjacent attention achieves the best results. We observe that adjacent design is more effective than global operation, whether using attention or using Concatenation&Conv. Besides, compared to concatenation and convolution, our AFFM, which is based on the attention mechanism, performs better. Lastly, global attention and the larger BEV encoder introduce more model parameters and achieve worse performance than pair-wise attention. This demonstrates that the performance improvements in pair-wise attention come from the design itself rather than the increased model parameters.

Independent BEV Feature Encoding. As analyzed in Sec.4.4, 3D object detection and BEV semantic segmentation tasks prefer different BEV feature grid sizes. As shown in Table 8, experimental results show that using BEV feature maps in different sizes for different tasks achieves the best multi-task performance trade-off. Moreover, adopting independent adaptive feature selection and BEV encoder for each task can further improve the multi-task performance of 1.7 NDS, 1.1 mAP, and 3.4 mIoU.

Table 7: Ablation of Temporal Feature Integration module. Our proposed backward and forward processes with AFFM achieve the best results.

Temporal Integration	NDS	mAP	Parameters
Global Concatenation&Conv (BEVDepth4D [11])	52.3	40.8	76.51M
Global Concatenation&Conv + larger BEV encoder	52.4	40.7	77.70M
Global attention	52.6	40.9	76.68M
Forward with adjacent Concatenation&Conv	52.8	40.6	76.63M
Forward with AFFM	53.1	41.2	76.64M
Backward + Forward with adjacent Concatenation&Conv	52.8	40.7	76.63M
Backward + Forward with AFFM (Ours)	53.2	41.5	76.64M

Table 8: Ablation of Independent BEV Feature Encoding ‘AFS’ is the adaptive feature selection. ‘IE’ denotes the independent BEV encoder. All experiments only used a single BEVDepth4D with ResNet-50 as the image encoder.

Det-grid	Seg-grid	AFS	IE	NDS	mAP	mIoU
0.4m	0.4m			53.2	41.9	41.6
0.8m	0.8m			50.5	39.6	50.9
0.4m	0.8m			52.9	42.0	50.6
0.4m	0.8m	✓		53.3 ↑0.4	42.3 ↑0.3	51.2 ↑0.6
0.4m	0.8m	✓	✓	54.6 ↑1.7	43.1 ↑1.1	54.0 ↑3.4

Table 9: Multi-task results under different loss weights.

α_{depth}	α_{cls}	α_{bbox}	α_{segveh}	$\alpha_{segarea}$	α_{segdiv}	NDS	mIoU	mIoU _v	mIoU _a	mIoU _d
1	2.5	6	100	100	100	60.0	57.3	47.5	81.4	43.1
1	2.5	6	180	45	90	59.7	57.6	49.1	81.1	42.6
1	2.5	6	300	70	200	59.9	58.0	49.5	81.3	43.4

Loss Weights. Table 9 shows how we adjust the loss weight to obtain the results in Table 1. Specifically, we follow BEVDepth [18] to set $\alpha_{depth} = 1$, $\alpha_{cls} = 1.5$, and $\alpha_{box} = 6$. We find that a larger segmentation loss weight achieves higher segmentation performance. Thus, we adjust the loss balance of each segmentation sub-task to obtain better overall segmentation results. The results show that carefully tuning loss weights can provide some improvement.

5 Conclusion

In this paper, we present HENet, an end-to-end framework for multi-task 3D perception. We propose a hybrid image encoding network and the temporal feature integration module to deal efficiently with high-resolution and long-term temporal image inputs. Besides, we adopt task-specific BEV grid sizes, independent BEV feature encoder and decoder to address multi-task conflict issue. Experimental results show that HENet obtains the state-of-the-art multi-task results on nuScenes, including 3D object detection and BEV semantic segmentation.

References

1. Badrinarayanan, V., Kendall, A., Cipolla, R.: Segnet: A deep convolutional encoder-decoder architecture for image segmentation. *IEEE TPAMI* (2017)
2. Brazil, G., Liu, X.: M3d-rpn: Monocular 3d region proposal network for object detection. In: *ICCV* (2019)
3. Caesar, H., Bankiti, V., Lang, A.H., Vora, S., Lioung, V.E., Xu, Q., Krishnan, A., Pan, Y., Baldan, G., Beijbom, O.: nuscenes: A multimodal dataset for autonomous driving. In: *CVPR* (2020)
4. Ding, M., Huo, Y., Yi, H., Wang, Z., Shi, J., Lu, Z., Luo, P.: Learning depth-guided convolutions for monocular 3d object detection. In: *CVPR* (2020)
5. Feng, C., Jie, Z., Zhong, Y., Chu, X., Ma, L.: Aedet: Azimuth-invariant multi-view 3d object detection. In: *CVPR*. pp. 21580–21588 (2023)
6. He, K., Zhang, X., Ren, S., Sun, J.: Deep residual learning for image recognition. In: *CVPR* (2016)
7. Hu, A., Murez, Z., Mohan, N., Dudas, S., Hawke, J., Badrinarayanan, V., Cipolla, R., Kendall, A.: Fiery: Future instance prediction in bird's-eye view from surround monocular cameras. In: *ICCV* (2021)
8. Hu, Y., Yang, J., Chen, L., Li, K., Sima, C., Zhu, X., Chai, S., Du, S., Lin, T., Wang, W., Lu, L., Jia, X., Liu, Q., Dai, J., Qiao, Y., Li, H.: Planning-oriented autonomous driving. In: *CVPR* (2023)
9. Huang, B., Li, Y., Xie, E., Liang, F., Wang, L., Shen, M., Liu, F., Wang, T., Luo, P., Shao, J.: Fast-bev: Towards real-time on-vehicle bird's-eye view perception. *arXiv preprint arXiv:2301.07870* (2023)
10. Huang, J., Huang, G.: Bevpoolv2: A cutting-edge implementation of bevdet toward deployment. *arXiv preprint arXiv:2211.17111* (2022)
11. Huang, J., Huang, G., Robotics, P.: Bevdet4d: Exploit temporal cues in multi-camera 3d object detection. *arXiv preprint arXiv:2203.17054* (2022)
12. Huang, J., Huang, G., Zhu, Z., Ye, Y., Du, D.: Bevdet: High-performance multi-camera 3d object detection in bird-eye-view. *arXiv preprint arXiv:2112.11790* (2021)
13. Jiang, X., Li, S., Liu, Y., Wang, S., Jia, F., Wang, T., Han, L., Zhang, X.: Far3d: Expanding the horizon for surround-view 3d object detection. In: *AAAI* (2024)
14. Jiang, Y., Zhang, L., Miao, Z., Zhu, X., Gao, J., Hu, W., Jiang, Y.G.: Polarformer: Multi-camera 3d object detection with polar transformer. In: *AAAI*. pp. 1042–1050 (2023)
15. Lee, Y., Park, J.: Centermask: Real-time anchor-free instance segmentation. In: *CVPR* (2020)
16. Li, Q., Wang, Y., Wang, Y., Zhao, H.: Hdmapnet: An online hd map construction and evaluation framework. In: *ICRA* (2022)
17. Li, Y., Bao, H., Ge, Z., Yang, J., Sun, J., Li, Z.: Bevstereo: Enhancing depth estimation in multi-view 3d object detection with dynamic temporal stereo. In: *AAAI* (2023)
18. Li, Y., Ge, Z., Yu, G., Yang, J., Wang, Z., Shi, Y., Sun, J., Li, Z.: Bevdepth: Acquisition of reliable depth for multi-view 3d object detection. In: *AAAI* (2023)
19. Li, Z., Wang, W., Li, H., Xie, E., Sima, C., Lu, T., Qiao, Y., Dai, J.: Bevformer: Learning bird's-eye-view representation from multi-camera images via spatiotemporal transformers. In: *ECCV* (2022)
20. Li, Z., Yu, Z., Wang, W., Anandkumar, A., Lu, T., Alvarez, J.M.: Fb-bev: Bev representation from forward-backward view transformations. In: *ICCV*. pp. 6919–6928 (2023)

21. Liang, T., Xie, H., Yu, K., Xia, Z., Lin, Z., Wang, Y., Tang, T., Wang, B., Tang, Z.: Bevfusion: A simple and robust lidar-camera fusion framework. In: NeurIPS (2022)
22. Lin, T.Y., Dollár, P., Girshick, R., He, K., Hariharan, B., Belongie, S.: Feature pyramid networks for object detection. In: CVPR (2017)
23. Lin, T.Y., Goyal, P., Girshick, R., He, K., Dollár, P.: Focal loss for dense object detection. In: ICCV (2017)
24. Lin, X., Lin, T., Pei, Z., Huang, L., Su, Z.: Sparse4d: Multi-view 3d object detection with sparse spatial-temporal fusion. arXiv preprint arXiv:2211.10581 (2022)
25. Lin, X., Lin, T., Pei, Z., Huang, L., Su, Z.: Sparse4d v2: Recurrent temporal fusion with sparse model. arXiv preprint arXiv:2305.14018 (2023)
26. Liu, H., Teng, Y., Lu, T., Wang, H., Wang, L.: Sparsebev: High-performance sparse 3d object detection from multi-camera videos. In: ICCV (2023)
27. Liu, Y., Wang, T., Zhang, X., Sun, J.: Petr: Position embedding transformation for multi-view 3d object detection. In: ECCV (2022)
28. Liu, Y., Yan, J., Jia, F., Li, S., Gao, A., Wang, T., Zhang, X.: Petrv2: A unified framework for 3d perception from multi-camera images. In: ICCV (2023)
29. Nicolas, C., Francisco, M., Gabriel, S., Nicolas, U., Alexander, K., Sergey, Z.: End-to-end object detection with transformers. In: ECCV (2020)
30. Pan, B., Sun, J., Leung, H.Y.T., Andonian, A., Zhou, B.: Cross-view semantic segmentation for sensing surroundings. IEEE Robotics and Automation Letters (2020)
31. Park, D., Ambrus, R., Guizilini, V., Li, J., Gaidon, A.: Is pseudo-lidar needed for monocular 3d object detection? In: ICCV (2021)
32. Park, J., Xu, C., Yang, S., Keutzer, K., Kitani, K., Tomizuka, M., Zhan, W.: Time will tell: New outlooks and a baseline for temporal multi-view 3d object detection. In: ICLR (2023)
33. Philion, J., Fidler, S.: Lift, splat, shoot: Encoding images from arbitrary camera rigs by implicitly unprojecting to 3d. In: ECCV (2020)
34. Reading, C., Harakeh, A., Chae, J., Waslander, S.L.: Categorical depth distribution network for monocular 3d object detection. In: CVPR. pp. 8555–8564 (2021)
35. Roddick, T., Cipolla, R.: Predicting semantic map representations from images using pyramid occupancy networks. In: CVPR (2020)
36. Roddick, T., Kendall, A., Cipolla, R.: Orthographic feature transform for monocular 3d object detection. arXiv preprint arXiv:1811.08188 (2018)
37. Wang, S., Liu, Y., Wang, T., Li, Y., Zhang, X.: Exploring object-centric temporal modeling for efficient multi-view 3d object detection. In: ICCV (2023)
38. Wang, T., Pang, J., Lin, D.: Monocular 3d object detection with depth from motion. In: ECCV (2022)
39. Wang, T., Zhu, X., Pang, J., Lin, D.: Fcos3d: Fully convolutional one-stage monocular 3d object detection. In: ICCV (2021)
40. Wang, Y., Chao, W.L., Garg, D., Hariharan, B., Campbell, M., Weinberger, K.Q.: Pseudo-lidar from visual depth estimation: Bridging the gap in 3d object detection for autonomous driving. In: CVPR. pp. 8445–8453 (2019)
41. Wang, Y., Guizilini, V., Zhang, T., Wang, Y., Zhao, H., Solomon, J.: Detr3d: 3d object detection from multi-view images via 3d-to-2d queries. In: CoRL (2021)
42. Wang, Z., Min, C., Ge, Z., Li, Y., Li, Z., Yang, H., Huang, D.: Sts: Surround-view temporal stereo for multi-view 3d detection. arXiv preprint arXiv:2208.10145 (2022)

43. Xie, E., Yu, Z., Zhou, D., Phlion, J., Anandkumar, A., Fidler, S., Luo, P., Alvarez, J.M.: M2bev: Multi-camera joint 3d detection and segmentation with unified birds-eye view representation. arXiv preprint arXiv:2204.05088 (2022)
44. Yang, C., Chen, Y., Tian, H., Tao, C., Zhu, X., Zhang, Z., Huang, G., Li, H., Qiao, Y., Lu, L., et al.: Bevformer v2: Adapting modern image backbones to bird's-eye-view recognition via perspective supervision. In: CVPR. pp. 17830–17839 (2023)
45. Yang, W., Li, Q., Liu, W., Yu, Y., Ma, Y., He, S., Pan, J.: Projecting your view attentively: Monocular road scene layout estimation via cross-view transformation. In: CVPR (2021)
46. Yang, Z., Zhou, Y., Chen, Z., Ngiam, J.: 3d-man: 3d multi-frame attention network for object detection. In: CVPR. pp. 1863–1872 (2021)
47. Yin, T., Zhou, X., Krahenbuhl, P.: Center-based 3d object detection and tracking. In: CVPR (2021)
48. Yuan, Y., Huang, L., Guo, J., Zhang, C., Chen, X., Wang, J.: Ocnet: Object context network for scene parsing. arXiv preprint arXiv:1809.00916 (2018)
49. Zhang, Y., Zheng, W., Zhu, Z., Huang, G., Lu, J., Zhou, J.: A simple baseline for multi-camera 3d object detection. In: AAAI. pp. 3507–3515 (2023)
50. Zhou, B., Krähenbühl, P.: Cross-view transformers for real-time map-view semantic segmentation. In: CVPR (2022)
51. Zhu, B., Jiang, Z., Zhou, X., Li, Z., Yu, G.: Class-balanced grouping and sampling for point cloud 3d object detection. arXiv preprint arXiv:1908.09492 (2019)
52. Zhuang, Z., Li, R., Jia, K., Wang, Q., Li, Y., Tan, M.: Perception-aware multi-sensor fusion for 3d lidar semantic segmentation. In: ICCV (2021)
53. Zong, Z., Jiang, D., Song, G., Xue, Z., Su, J., Li, H., Liu, Y.: Temporal enhanced training of multi-view 3d object detector via historical object prediction. In: ICCV (2023)